Proceedings of the
9th Graz Brain-Computer Interface Conference 2024
10.3217/978-3-99161-014-4-053

MAPPING NEUROMUSCULAR REPRESENTATION OF GRASPING MOVEMENTS USING ULTRA-HIGH-DENSITY EEG AND EMG

Leonhard Schreiner[1,2*], Pauline Schomaker[4*], Sebastian Sieghartsleitner[1,3], Michael Schwarzgruber[1], Harald Pretl[2], Andreea I. Sburlea[4], Christoph Guger[1]

[1] g.tec medical engineering GmbH, Schiedlberg, Austria
[2] Institute for Integrated Circuits, Johannes Kepler University, Linz, Austria
[3] Institute of Computational Perception, Johannes Kepler University, Linz, Austria
[4] Bernoulli Institute for Mathematics, Computer Science and Artificial Intelligence, University of Groningen, the Netherlands

E-mail: schreiner@gtec.at
*These authors contributed equally to this work.

ABSTRACT: Understanding the intricate coordination between the brain and muscles during movement tasks is crucial for advancing our knowledge of motor control and enhancing Brain-Computer Interface (BCI) devices. This study investigates the mechanisms underlying grasping movements using diverse objects and grasping techniques. Employing a novel ultra-high-density (uHD) EEG/EMG system, the study examines neural and muscular activity with high spatial resolution. Results of three healthy subjects highlight event-related desynchronization/synchronization (ERD/S) patterns and classification accuracies for EEG and EMG signals during grasping tasks. Temporal analysis reveals a strong relationship between EMG/EEG activation and classification outcomes, supported by kinematic data as evidence of motion. S02 achieved the highest average EEG and EMG classification accuracies at 69.4% and 97.8%, respectively, while S01 had the lowest at 64% and 85.4%. The observed dependencies between accuracies imply an interconnected and synergistic relationship between EEG and EMG modalities, which holds promise for enhancing overall performance in future BCIs.

INTRODUCTION

Examining our brain's and muscles' coordination during movement tasks elucidates the intricate mechanisms underlying motor control. The primary aim of this study is to investigate the grasping of objects, including a multitude of grasp types and objects, to enhance future brain-computer interface (BCI) devices. Researchers have explored the mechanics of grasping in both animals and humans using various methodologies [1], [2], [3], [4], [5], [6], [7]. Nonetheless, a substantial gap in knowledge remains regarding the precise mechanisms through which our brains govern these movements, particularly as they evolve. Non-invasive techniques such as EEG offer high temporal resolution, allowing for studying neural dynamics during grasping. However, their spatial resolution is often limited, constraining the capacity to attain a more nuanced comprehension of neural control [8], [9], [10], [11]. Similarly, EMG devices, often characterized by low resolution [12], are used to investigate muscular activities. Our research utilizes a novel ultra-high-density (uHD) EEG/EMG system to explore the intricate interplay between neural and muscular activity in greater spatial detail. The system demonstrates improvements due to its increased sensor density, outperforming other high-density EEG systems. It has been effectively utilized in research studies focused on decoding finger movements [11], hand gestures [14], and mapping the central sulcus using somatosensory evoked potentials [13].

We aim to expand the scope of discrimination by employing various objects and grasping types, thus delving into multiple dimensions for precise analysis. Sburlea et al. [3] investigated the slow-frequency EEG components with a similar paradigm. They found that the grasp types are encoded in motor cortex areas, while object properties activate the frontoparietal regions. Additionally, they discovered that the grasp types are significantly better decoded during the execution and release stages than the observation stage. Building upon their findings, we focus our investigations on the motor cortex area contralateral to the moved hand in the execution and release stages. However, we focused on extracting EEG frequencies in the 8-30 Hz range, which are substantial in movement decoding in EEG research [14], [15].

MATERIALS AND METHODS

Our system incorporates flexible surface electrode grids that were applied on the scalp as well as arm, and hand muscles. The uHD EEG/EMG system (g.Pangolin, g.tec medical engineering GmbH, Austria) has an inter-electrode distance of 8.6 mm and an exposed sensor diameter of 5.9 mm. We used the system to measure data from three healthy subjects (two right-handed and one left-handed).

Published by
Verlag der Technischen Universität Graz

10.3217/978-3-99161-014-4-053

Two biosignal amplifiers (see Fig. 1A(a)) allow the acquisition of an average amount (across subjects) of 330 channels of biosignal data, with an average of 235 channels dedicated to scalp recordings (176 (S01), 256 (S02), and 272 (S03)). We recorded EMG data from 96 channels across all subjects, focusing on intrinsic (hand) and extrinsic (forearm) arm muscles. (see Fig. 1A). Data was acquired with a sample rate of 512 Hz. Additionally, the kinematics of the hand and arm movements are acquired and digitized using the leap motion camera [16] at a variable sample rate between 80 and 120 Hz. The grasping task and six different grasps are visible in Fig. 1 B. We distinguished between four objects (big sphere, small sphere, big cylinder, small cylinder) and three grasping types (power, precision, pinch), resulting in a total of 12 grasping conditions, as demonstrated by Sburlea et al. [3]. Each grasping type was executed 27 times per object per run. Two runs per object were performed, with randomized order, resulting in 54 trials for further analysis. Additionally, within each run, the grasping types were shuffled.

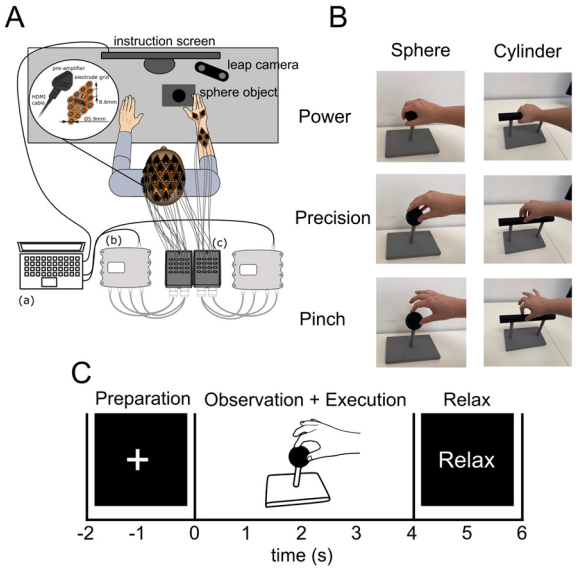

Figure 1: uHD EEG/EMG system for decoding object grasping task. (A) schematic system setup: two g.HIamp (b) (g.tec medical engineering GmbH) biosignal amplifiers, each with 256 channels, connected to the acquisition computer (a) for synchronous EEG and EMG recording. The uHD EEG system comprises electrode grids with 16 channels and a pre-amplifier attached to each grid, connected to the connector box (c). For EEG acquisition, an average of 235 channels covers sensory and motor areas on the contralateral hemispheres. Six grids (96 channels) are placed on the extrinsic and intrinsic hand muscles for EMG data acquisition. (B) Two objects (small sphere, small cylinder) and three grasp types (power, precision, and pinch) are depicted; see [3] for all 12 classes of the object grasps. (C) Paradigm Procedure: The procedure commences with the display of a fixation cross for 2 seconds, followed by randomized instructions for the grasping task (4 seconds), succeeded by a 2-second relaxation period.

Subjects are then directed to prepare for the next 8-second cycle. In total, 54 trials per class were recorded. Instructions were given on a computer screen placed approximately 1.5 meters in front of the subjects. First, a fixation cross was displayed for 2 seconds, followed by a 4-second observation and execution phase, during which pictures depicting the object and grasp to be performed were presented, as illustrated in Fig. 1B. Subsequently, upon completing the grasping task, participants were instructed to return to the starting position, relax their arm/hand, and prepare for the upcoming trial (Fig. 1C).

EEG Preprocessing

The raw EEG recordings were first notch-filtered at 50 Hz and its harmonics using a 2nd-order Butterworth filter. After notch-filtering, bad channels were identified and removed using the approach described in [11], except for the band-pass filter ranging from 0.5 to 40 Hz instead. Finally, EEG data were common average referenced.

Feature Extraction and Epoching

For the classification of grasp types, band power features based on 8 to 30 Hz (4th-order Butterworth band-pass filter) were extracted as this frequency range encompasses both mu (8-12 Hz) and beta (13-30 Hz) rhythms which are associated with motor functions [17], [18]. Note that mu and beta rhythms may be analyzed separately. However, this was not done for the current classification analysis to keep dimensionality (i.e., number of features) low. On the other hand, beta band power features were extracted for topography plots.

The band power was estimated by squaring EEG time samples and applying a centered moving average using a window length of 0.75 seconds and a step size of 0.1 seconds. Furthermore, band power estimates were log-transformed to improve Gaussianity (i.e., normality) [19]. Finally, the log-transformed band power features were epoched using 1-second pre- and 8 second post-cue.

EEG Classification

Classification models were employed to investigate if the extracted band power features can differentiate between the grasp types. Specifically, pairwise classification of grasp types was performed for each object, respectively, leading to 12 two-class classification problems per subject. Pairwise classification was employed instead of a 3-class problem to allow for easier interpretation of results. Note that a classification analysis between objects was not carried out as objects were not shuffled on a trial-by-trial basis, which would lead to inflated accuracies due to the non-stationarity observed in EEG.

A regularized linear discriminant analysis (rLDA) was utilized as a classification model, with the regularization parameter α set to 0.1 [20]. The classification framework used was a 10-times 10-fold cross-validation, in which the random seed was set to the respective iteration (i.e., 1 to 10) to allow for reproducible results.

Topography Plots

Topography plots were created according to [11] and [21] using a custom montage creator software (g.tec medical engineering GmbH, Austria). Event-related desynchronization/synchronization (ERD/S) was

Published by
Verlag der Technischen Universität Graz

10.3217/978-3-99161-014-4-053

calculated using the log-transformed band power features of the beta band, with the baseline reflecting 0.5 seconds pre-cue. The brain models depicted in the topography plots were created using anatomical MRI scans from all participants. The brain and skull were reconstructed using FreeSurfer software (developed at the Martinos Center for Biomedical Imaging in Cambridge, MA, United States) based on the T1-weighted MRI data [22].

EMG

The raw EMG recordings were notch-filtered at 50 Hz and its harmonics, using a 2nd-order Butterworth filter. EMG features reflected simple root-mean-square values (RMS) of the band-pass filtered EMG (20 to 200 Hz, 4th-order Butterworth filter) data. The window length and step size were set to 0.2 and 0.05 seconds, respectively. Finally, RMS features were epoched using 1 second pre- and 8 second post-cue.

MVC

Maximum Voluntary Contraction (MVC) was recorded using a commercially available dynamometer. Participants performed a maximum contraction with their dominant hand for five seconds, followed by a one-minute break. The contraction was repeated three times and was performed by using a power grip on the dynamometer. The EMG signals obtained during MVC were then used to normalize EMG signals obtained during the grasping paradigm [23].

EMG Classification

EMG classification of grasps per object was analogous to EEG classification, except that 3-class classification for the grasp types was performed and that α was set to 0.25 for the rLDA. Thus, four classification problems, one for each object, were carried out per subject. The three-class classification was carried out as EMG is expected to result in much greater accuracy and, thus, easier interpretable results.

RESULTS

Fig. 2 illustrates the ERD/S topographies from all subjects, with the time points set to 1 second (for S01 and S02) and 1.5 seconds (for S03) after task instruction, as these time points reveal the most pronounced ERD for all subjects, respectively. The large and small object conditions were averaged for each grasp type, resulting in 6 conditions. During the sphere power grasp, S01 and S02 exhibited the most significant ERD at the contralateral hemisphere, around the C3 and C4 electrode positions, for S02 and S01 respectively. S03 showed the greatest consistency across all objects and grasps and demonstrated a clear focal spot around the C1 and C3 electrode positions. In other words, S01 and S02 exhibit more lateralized ERD, whereas S03's ERD is slightly more central. A weaker ERD was observed for S01, and the sphere object led to a stronger ERD than the cylinder.

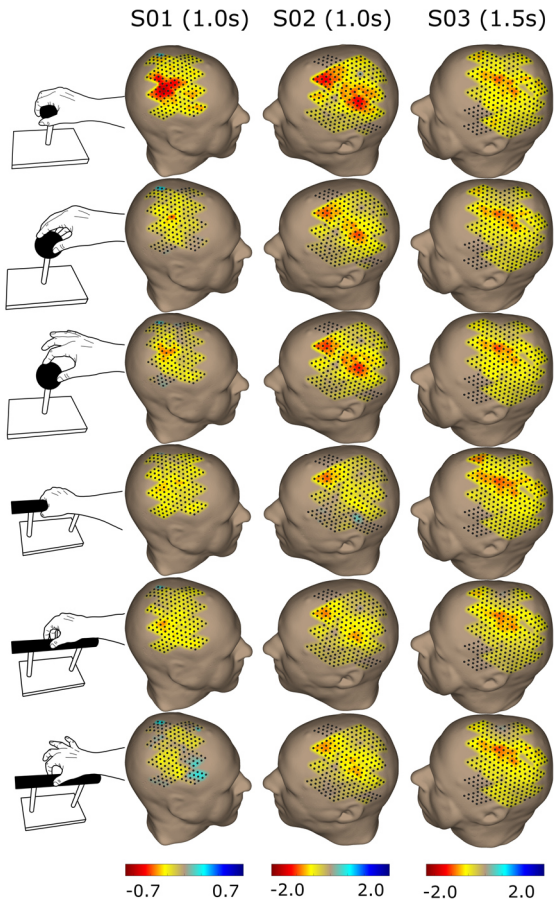

Figure 2: ERD/S Topographical maps were created for each participant and the corresponding grasping type. The hemispheres are shown contralateral to the hand-side of the grasp, with S01 being left-handed and S02 and S03 right-handed. The maps were constructed utilizing the beta frequency range (13-30 Hz) at 1 second for S01 and S02 and 1.5 seconds for S03—values in dB.

Fig. 3 shows the topographical ERD/S time course obtained for the beta frequency band features, averaged over both sphere objects (big and small), and power grasps for subject S03. The time window was set to -1 s pre-task instruction and 8 s post-task instruction (1 s steps) for a detailed temporal representation. The representation of the EMG RMS power for the same tasks was separated into intrinsic (blue) and extrinsic (green) muscles and depicted as mean (SD). The EMG RMS filtered from 20-200 Hz was calculated as a percentage according to the MVC measurement. The data from the leap motion camera was used for kinematic analysis. The retrieved velocity of the vertical movement from the hand/arm is depicted as mean (SD) in m/s (magenta). The EEG Accuracy graph in the last row (orange) is calculated in 0.1 s steps as mean (SD) for the ten runs from the 10 times 10-fold cross-validation. The EMG accuracy graph (cyan) reflects the outcome of a 3-lass problem. Similar to the EEG classification, the mean (SD) from the ten classification runs was plotted. Empirical chance levels were obtained by generating null models in which the class labels were shuffled and marked as dashed lines in Fig. 3.

Published by
Verlag der Technischen Universität Graz

10.3217/978-3-99161-014-4-053

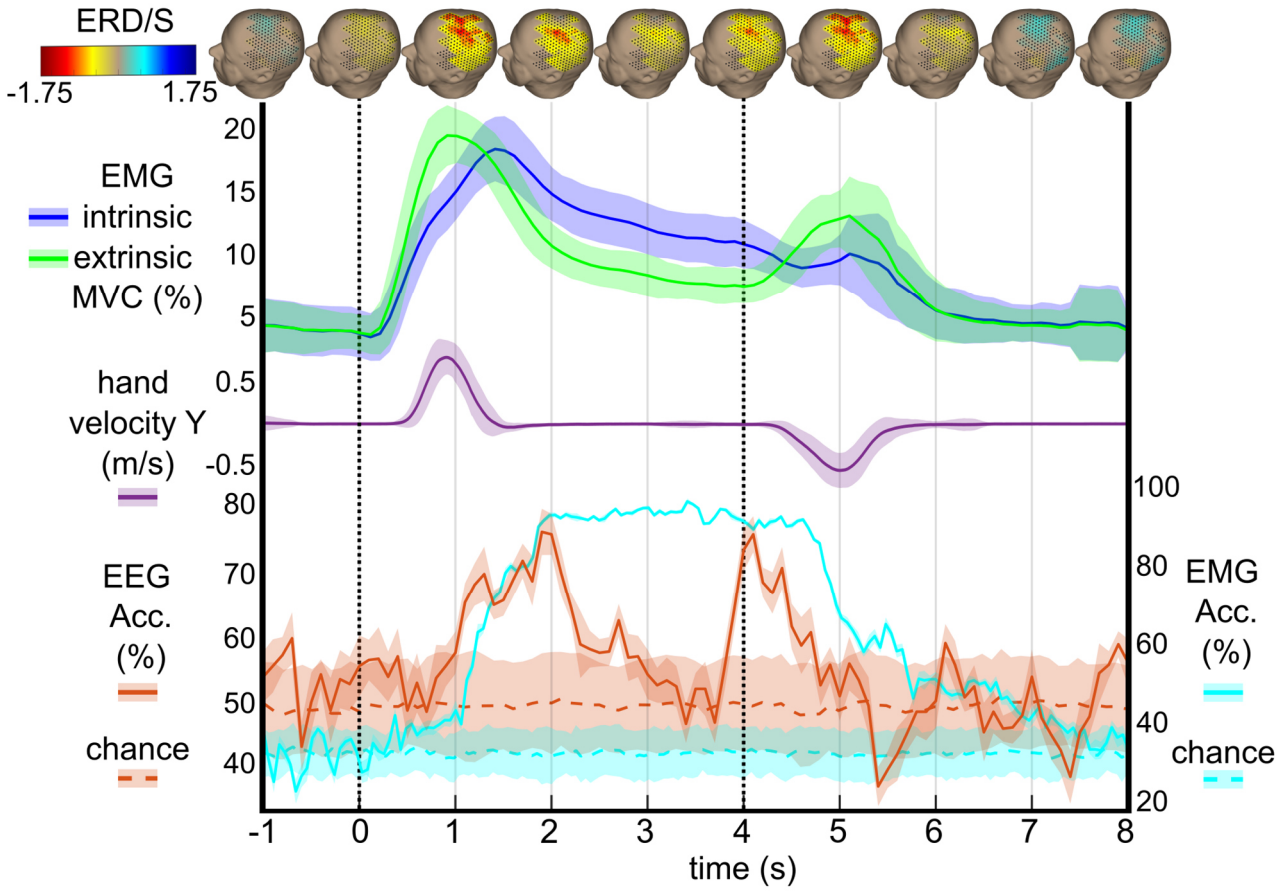

Figure 3: Subject S03 detailed analysis of the sphere power condition (small / big sphere merged). The time axis ranges from -1 to 8 seconds, with 0 as the task presentation on screen and the relax instruction at 4 seconds. The first row shows the ERD/S topographical time course. The maps were constructed utilizing the beta frequency band (13-30 Hz) with power shown in dB (color bar encodes ERD in red and ERS in blue). Row 2 represents the EMG MVC (%) time course from the 20-200 Hz filtered RMS signal as mean (SD) in blue for the intrinsic muscles and green for the extrinsic hand muscles. Row 3 depicts the kinematics of the arm movement as Velocity (m/s) in vertical (Y) direction (lifting/lowering) as mean (SD) in magenta. The last row represents the classification accuracy for EEG big sphere power vs. precision (orange) and the EMG accuracies for the 3-class problem classification outcome for the big sphere object (cyan). The EEG axis scaling was set to 40-80% (left side), whereas the EMG Accuracies are drawn from 20–100% (right side). Real chance levels drawn as dashed lines: EEG (orange) and EMG (cyan).

Table 1: EEG Accuracies for all classification pairs

Grasps / Subjects		S01	S02	S03
Big Sph.	Power vs. Precision	47.9%	69.4%	**76.9%**
	Power vs. Pinch	63.5%	61.1%	70.4%
	Precision vs. Pinch	57.3%	57.4%	66.7%
Big Cyl.	Power vs. Precision	65.6%	**78.7%**	63.9%
	Power vs. Pinch	55.2%	74.1%	70.4%
	Precision vs. Pinch	**77.1%**	71.3%	64.8%
Sm. Sph.	Power vs. Precision	58.3%	76.9%	69.4%
	Power vs. Pinch	69.8%	74.1%	66.7%
	Precision vs. Pinch	67.7%	64.8%	57.4%
Sm. Cyl.	Power vs. Precision	66.7%	65.7%	71.3%
	Power vs. Pinch	72.9%	75.9%	75.0%
	Precision vs. Pinch	65.6%	63.9%	67.6%

Tab. 1 shows the pairwise EEG classification accuracies of all the grasping techniques across objects. For each subject, 12 accuracies are depicted. The classification pair with the highest averaged accuracy was found for Small Cylinder Power vs. Pinch with 74.6% across subjects. Subject S02 reached the highest average accuracy of 69.4% for all pairs, S03 reached 68.4%, and S01 had the lowest accuracy of 64%.

Table 2: EMG accuracies for 3-class problems

Grasps / Subjects	S01	S02	S03
Big Sph.	90.4%	97.7%	96.4%
Big Cyl.	98.1%	**98.8%**	95.9%
Sm. Sph.	**100%**	98.6%	98.1%
Sm. Cyl.	53.1%	96.2%	**99.4%**

Tab. 2 shows the EMG classification accuracies computed as 3-class problems (all grasping types included). The object with the best accuracy was the small sphere, with an average accuracy of 98.9% across subjects. The subject with the highest accuracy is similar to EEG S02, with 97.8% across objects. S02 reached 97.5%, and S01 has the lowest average accuracy of 85.4%.

Published by
Verlag der Technischen Universität Graz

10.3217/978-3-99161-014-4-053

DISCUSSION

As illustrated in Fig. 2 and Fig. 3, the uHD EEG system's high spatial resolution enables a thorough examination of ERD/S topographies. The spatiotemporal dynamics of ERD/S offer valuable insights into the brain patterns triggered by grasping movements and their neural representation. In Fig. 3 (top row), a desynchronization occurs at the time point (1s) after task instruction, declining from seconds 2-3, followed by another increase towards the offset of the grasping task. Following the ERD, an ERS becomes apparent 2 to 3 seconds after the movement termination. The topographies show a similar focal spot as found in prior studies using the uHD EEG system [11], [15] and other studies examining temporal ERD/S dynamics [24].

The EMG results from the intrinsic and extrinsic muscles have a similar temporal pattern (see Fig. 3) with an activation start around 200 ms after task instruction. However, the extrinsic group shows a steeper ascent of the curve and a slightly higher MVC percentage value at the beginning of the movement, which can be explained by a temporal difference in the activation of the muscles, meaning lifting off the arm incorporates more extrinsic muscles [25]. This is also reflected in the peak values, which reach around 1 second for extrinsic muscles and 1.4 seconds for intrinsic muscles. The intrinsic muscles show higher activation throughout the grasping task due to active grasping control and the possibility of slightly resting the arm on the object. When moving the arm back to the resting position, the extrinsic muscles show higher activation than the intrinsic. The results from the EMG analysis correspond closely with the temporal behavior observed in the data from the Leap camera, indicating a parallel trend in their patterns over time, with a slightly longer delay of approx. 0.5 seconds from task instruction to velocity onset can be explained by prior muscle activation and real movement detected by the camera. The EEG and EMG accuracy traces (Fig. 2 last row) started to incline from the chance level at around 1 second after task instruction, which is closely associated with the temporal behavior of the EMG and kinematics, however showing an additional 0.5 seconds delay for the movement onset [26]. The maximum EMG accuracy is stable at around the maximum of 95%; however, in comparison, the EEG accuracy declines again after the initial peak. This phenomenon may be attributed to diminished attention towards movement execution, as automatic patterns governed by lower-level brain structures entail reduced involvement of higher-order control mechanisms [27]. Interestingly, the EEG accuracy shows a second increase at the movement offset but peaks earlier than the movement onset. This temporal phenomenon could stem from anticipating returning the arm to the starting position [28].

S02 reached the highest accuracy for EEG and EMG classification with 69.4% and 97.8%, respectively (see Tab.1 and Tab. 2). S01 achieved the worst accuracy with 64% for EEG and 85.4% for EMG classification. Considering that S01 has the lowest amount of scalp channels used for classification, it also indicates that the high spatial density of EEG electrodes is beneficial for decoding motor tasks. A similar analysis was done by [11] using the uHD EEG, where they showed that when subsampling the electrode count, there was a decrease in accuracy for decoding individual finger movements. A lower ERD power was also observed for S01, which adds to the lower performance. For EMG, only the small sphere object grasp for S01 showed lower accuracies, which could be attributed to the removal of roughly half of the trials due to technical issues in the acquisition. The observed trend of superior performance in both EEG and EMG across subjects suggests a nuanced interplay between the examined modalities. This pattern highlights how the biosignals are interconnected and complement each other, suggesting they work synergistically to produce a combined effect greater than the sum of their individual contributions. Consequently, future research endeavors should prioritize utilizing parameters such as corticomuscular coherence alongside advanced classification methodologies to optimize the performance and functionality of brain-computer interfaces (BCIs) and neuroprosthetic systems.

Acknowledgements

The authors would like to thank the Institute of Neural Engineering, Graz University of Technology, for providing the objects for this study.

REFERENCES

[1] J. A. Michaels and H. Scherberger, ‘Population coding of grasp and laterality-related information in the macaque fronto-parietal network’, *Sci Rep*, vol. 8, no. 1, p. 1710, Jan. 2018, doi: 10.1038/s41598-018-20051-7.

[2] S. Schaffelhofer and H. Scherberger, ‘Object vision to hand action in macaque parietal, premotor, and motor cortices’, *eLife*, vol. 5, p. e15278, Jul. 2016, doi: 10.7554/eLife.15278.

[3] A. I. Sburlea, M. Wilding, and G. R. Müller-Putz, ‘Disentangling human grasping type from the object’s intrinsic properties using low-frequency EEG signals’, *Neuroimage: Reports*, vol. 1, no. 2, p. 100012, Jun. 2021, doi: 10.1016/j.ynirp.2021.100012.

[4] A. I. Sburlea and G. R. Müller-Putz, ‘Exploring representations of human grasping in neural, muscle and kinematic signals’, *Sci Rep*, vol. 8, no. 1, Art. no. 1, Nov. 2018, doi: 10.1038/s41598-018-35018-x.

[5] R. D. Flint, J. M. Rosenow, M. C. Tate, and M. W. Slutzky, ‘Continuous decoding of human grasp kinematics using epidural and subdural signals’, *J Neural Eng*, vol. 14, no. 1, p. 016005, Feb. 2017, doi: 10.1088/1741-2560/14/1/016005.

[6] G. Lange, C. Y. Low, K. Johar, F. A. Hanapiah, and F. Kamaruzaman, ‘Classification of

Published by
Verlag der Technischen Universität Graz

10.3217/978-3-99161-014-4-053

Electroencephalogram Data from Hand Grasp and Release Movements for BCI Controlled Prosthesis', *Procedia Technology*, vol. 26, pp. 374–381, Jan. 2016, doi: 10.1016/j.protcy.2016.08.048.

[7] A. Schwarz, P. Ofner, J. Pereira, A. I. Sburlea, and G. R. Müller-Putz, 'Decoding natural reach-and-grasp actions from human EEG', *J. Neural Eng.*, vol. 15, no. 1, p. 016005, Dec. 2017, doi: 10.1088/1741-2552/aa8911.

[8] A. K. Robinson, P. Venkatesh, M. J. Boring, M. J. Tarr, P. Grover, and M. Behrmann, 'Very high density EEG elucidates spatiotemporal aspects of early visual processing', *Sci Rep*, vol. 7, no. 1, p. 16248, Dec. 2017, doi: 10.1038/s41598-017-16377-3.

[9] C. M. Michel and D. Brunet, 'EEG Source Imaging: A Practical Review of the Analysis Steps', *Front Neurol*, vol. 10, p. 325, 2019, doi: 10.3389/fneur.2019.00325.

[10] V. Brodbeck *et al.*, 'Electroencephalographic source imaging: a prospective study of 152 operated epileptic patients', *Brain*, vol. 134, no. 10, pp. 2887–2897, Oct. 2011, doi: 10.1093/brain/awr243.

[11] H. S. Lee *et al.*, 'Individual finger movement decoding using a novel ultra-high-density electroencephalography-based brain-computer interface system', *Front Neurosci*, vol. 16, p. 1009878, Oct. 2022, doi: 10.3389/fnins.2022.1009878.

[12] M. Zia ur Rehman *et al.*, 'Multiday EMG-Based Classification of Hand Motions with Deep Learning Techniques', *Sensors*, vol. 18, no. 8, Art. no. 8, Aug. 2018, doi: 10.3390/s18082497.

[13] L. Schreiner *et al.*, 'Mapping of the central sulcus using non-invasive ultra-high-density brain recordings', *Sci Rep*, vol. 14, no. 1, p. 6527, Mar. 2024, doi: 10.1038/s41598-024-57167-y.

[14] G. Pfurtscheller, C. Neuper, D. Flotzinger, and M. Pregenzer, 'EEG-based discrimination between imagination of right and left hand movement', *Electroencephalography and clinical Neurophysiology*, vol. 103, no. 6, pp. 642–651, 1997, doi: 10.1016/S0013-4694(97)00080-1.

[15] L. Schreiner, S. Sieghartsleitner, K. Mayr, H. Pretl, and C. Guger, 'Hand gesture decoding using ultra-high-density EEG', in *2023 11th International IEEE/EMBS Conference on Neural Engineering (NER)*, Apr. 2023, pp. 01–04. doi: 10.1109/NER52421.2023.10123901.

[16] G. Marin, F. Dominio, and P. Zanuttigh, 'Hand gesture recognition with leap motion and kinect devices', in *2014 IEEE International Conference on Image Processing (ICIP)*, Paris, France: IEEE, Oct. 2014, pp. 1565–1569. doi: 10.1109/ICIP.2014.7025313.

[17] K. J. Miller, G. Schalk, E. E. Fetz, M. den Nijs, J. G. Ojemann, and R. P. N. Rao, 'Cortical activity during motor execution, motor imagery, and imagery-based online feedback', *Proceedings of the National Academy of Sciences*, vol. 107, no. 9, pp. 4430–4435, Mar. 2010, doi: 10.1073/pnas.0913697107.

[18] D. O. Cheyne, 'MEG studies of sensorimotor rhythms: a review', *Exp Neurol*, vol. 245, pp. 27–39, Jul. 2013, doi: 10.1016/j.expneurol.2012.08.030.

[19] J. Gruenwald, A. Znobishchev, C. Kapeller, K. Kamada, J. Scharinger, and C. Guger, 'Time-Variant Linear Discriminant Analysis Improves Hand Gesture and Finger Movement Decoding for Invasive Brain-Computer Interfaces', *Front. Neurosci.*, vol. 13, p. 901, Sep. 2019, doi: 10.3389/fnins.2019.00901.

[20] Y. Guo, T. Hastie, and R. Tibshirani, 'Regularized linear discriminant analysis and its application in microarrays', *Biostatistics*, vol. 8, no. 1, pp. 86–100, Jan. 2007, doi: 10.1093/biostatistics/kxj035.

[21] J. Kubanek and G. Schalk, 'NeuralAct: A Tool to Visualize Electrocortical (ECoG) Activity on a Three-Dimensional Model of the Cortex', *Neuroinformatics*, vol. 13, no. 2, pp. 167–174, Apr. 2015, doi: 10.1007/s12021-014-9252-3.

[22] A. M. Dale, B. Fischl, and M. I. Sereno, 'Cortical Surface-Based Analysis: I. Segmentation and Surface Reconstruction', *NeuroImage*, vol. 9, no. 2, pp. 179–194, Feb. 1999, doi: 10.1006/nimg.1998.0395.

[23] B. P. T. Ngo and R. P. Wells, 'Evaluating protocols for normalizing forearm electromyograms during power grip', *Journal of Electromyography and Kinesiology*, vol. 26, pp. 66–72, Feb. 2016, doi: 10.1016/j.jelekin.2015.10.014.

[24] G. Pfurtscheller, 'Functional brain imaging based on ERD/ERS', *Vision Research*, vol. 41, no. 10, pp. 1257–1260, May 2001, doi: 10.1016/S0042-6989(00)00235-2.

[25] C. I. Long, P. W. Conrad, E. A. Hall, and S. L. Furler, 'Intrinsic-Extrinsic Muscle Control of the Hand in Power Grip and Precision Handling: AN ELECTROMYOGRAPHIC STUDY', *JBJS*, vol. 52, no. 5, p. 853, Jul. 1970.

[26] E. Trigili *et al.*, 'Detection of movement onset using EMG signals for upper-limb exoskeletons in reaching tasks', *Journal of NeuroEngineering and Rehabilitation*, vol. 16, no. 1, p. 45, Mar. 2019, doi: 10.1186/s12984-019-0512-1.

[27] R. M. Hardwick, S. Caspers, S. B. Eickhoff, and S. P. Swinnen, 'Neural correlates of action: Comparing meta-analyses of imagery, observation, and execution', *Neuroscience & Biobehavioral Reviews*, vol. 94, pp. 31–44, Nov. 2018, doi: 10.1016/j.neubiorev.2018.08.003.

[28] P. Cisek and J. F. Kalaska, 'Neural Correlates of Reaching Decisions in Dorsal Premotor Cortex: Specification of Multiple Direction Choices and Final Selection of Action', *Neuron*, vol. 45, no. 5, pp. 801–814, Mar. 2005, doi: 10.1016/j.neuron.2005.01.027.

Published by
Verlag der Technischen Universität Graz